Opto-Electronics Review

journal homepage: https://journals.pan.pl/opelre

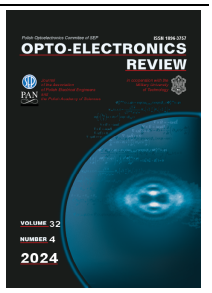


# Glass-ceramic materials: influence of fluoride nanocrystals on emission properties of lanthanide ions

Joanna Śmiarowska*, Natalia Pawlik, Joanna Pisarska, Wojciech A. Pisarski*

Institute of Chemistry, University of Silesia, ul. Szkolna 9, 40-007 Katowice, Poland

**Article info**

*Article history:*
Received 28 Jul. 2024
Received in revised form 24 Sep. 2024
Accepted 07 Oct. 2024
Available on-line 05 Nov. 2024

*Keywords*:
glass-ceramic materials;
lanthanide ions;
optical properties;
visible emission.

**Abstract**

In this work, the oxyfluoride glass-ceramic materials containing $LaF_3$ nanocrystals, prepared by using the sol-gel method, were described. The influence of fluoride nanocrystals on the photoluminescence properties of selected lanthanide ions was determined. The experimental results obtained for nano-glass-ceramics were compared to the precursor xerogels. Those $Ln^{3+}$-doped sol-gel materials with dispersed $LaF_3$ nanocrystals exhibit several visible emission bands. It was observed that heat-treatment process caused the elongation of the lifetimes of the $^5D_0$ state from $\tau = 0.22$ ms to $\tau_1 = 0.79$ ms, $\tau_2 = 9.76$ ms (for $Eu^{3+}$-doped materials) and of the $^4F_{9/2}$ state from $\tau = 0.027$ ms to $\tau_1 = 0.034$ ms, $\tau_2 = 1.731$ ms (for $Dy^{3+}$-doped materials). The performed studies clearly revealed that luminescence behaviour also depends on an activator concentration and a distribution of energy levels of lanthanide ions.

## 1. Introduction

Glass-ceramics (GCs) are considered as an intriguing group of modern materials, combining the unique features of both amorphous and crystalline media. The heat-treatment process carried out at controlled time and temperature conditions results in a formation of very interesting glass-ceramic materials in terms of various properties and applications. Dr S. Donald Stookey pioneered this research field [1] and George Beall progressively continued those studies [2–4]. Since then, many papers have been published on glass-ceramic systems and concentrate on their synthesis and structure [5–7], but also on commercialization fields and various, often multifunctional applications [8, 9]. The diversity of chemical compositions, the development of innovative synthesis methods, and the unique structures obtained at the nano/microscale have contributed to a renewed perspective on the definition of glass-ceramic materials [10].

Transparent glass-ceramic materials doped with lanthanide ions, capable of emitting irradiation in the visible, as well as near- and mid-infrared range, have gained significant interest in photonics, i.e., amplifiers [11], solid-state lasers [12–14], optical fibres [15], and up-conversion devices [16, 17]. Among GCs doped with $Ln^{3+}$ ions, the materials doped with $Eu^{3+}$, $Dy^{3+}$ and $Pr^{3+}$ exhibit interesting optical properties.

The transformation from glass to glass-ceramic results in an enhancement of luminescence bands and prolongation of the luminescence decay times of $Ln^{3+}$ ions [18]. Additionally, manipulating plentiful parameters, e.g., temperature and time of heat treatment of as-prepared glasses, their initial composition, or type of crystallized phase, allows for a successful tunability of $Re^{3+}$ resultant emission. Thus, $Eu^{3+}$-doped GCs can be successfully used as red-emitting components for white light emitted diodes (WLEDs) [19, 20] or in luminescence thermometry [21]. Further, $Dy^{3+}$-doped GCs are commonly utilized as white light emitters [22–24], but also – similarly as $Eu^{3+}$-doped GCs – in optical thermometry [25]. Finally, the luminescence features of $Pr^{3+}$-doped GCs predispose them to use as wide-range colour converters with for blue LEDs [26], as white-light-emitting fibre lasers [27] or in optical-fibre temperature sensing [28], as well as in down-conversion luminescence applications [29].

Among the numerous glass-ceramic materials, the oxyfluoride systems containing lanthanide ions deserve special attention. During initial glass or xerogel heat

*Corresponding authors at: wojciech.pisarski@us.edu.pl
joanna.smiarowska@us.edu.pl

https://doi.org/10.24425/opelre.2024.152680
1896-3757/ Association of Polish Electrical Engineers (SEP) and Polish Academic of Sciences (PAS). Published by PAS

treatment, the fluoride nanocrystals could successfully precipitate inside an amorphous oxide host matrix. Lanthanide ions are extensively used as optically active dopants and are typically present in both amorphous phase and crystalline fraction. As a result, the optical properties change significantly due to the partial alteration of the nearest surrounding around the lanthanide ion. In recent years, a series of oxyfluoride GCs containing $LaF_3$ nanocrystals (where $Ln^{3+}$ [Ln = Ho [30], Yb [31], Er [32–34], Nd [35, 36], Pr/Yb [37] ions partially replace $La^{3+}$ ones) have gained significant importance. Some of such systems were fabricated using the sol-gel method [38–40]. This paper refers to this issue. This research aimed to investigate the effect of $LaF_3$ nanocrystals dispersed in sol-gel materials on the emission properties of selected lanthanide ions.

The work concerned with performing a comparative analysis of photoluminescent features of silicate sol-gel materials singly-doped with $Eu^{3+}$, $Dy^{3+}$, and $Pr^{3+}$ ions, described by us earlier [41–43]. The aim of this work was to compile the conclusions, specifying how the diversity of the energy level structure, as well as differences in the ionic radii between $La^{3+}$ (from parent $LaF_3$ crystal phase) and individual active dopants determine the photoluminescent properties of the prepared sol-gel materials.

## 2. Experimental

The sol-gel preparation method was used to synthesize the xerogels doped with $Eu^{3+}$, $Dy^{3+}$, and $Pr^{3+}$ ions. To obtain the nano-glass-ceramic materials, the as-prepared xerogels were annealed at selected time and temperature conditions; the details were presented elsewhere [41, 42]. The solutions of La(III) and Eu(III), Dy(III), and Pr(III) acetates dissolved in water and trifluoroacetic acid (TFA) were added dropwise to the pre-hydrolysis mixtures containing tetraetoxysilane (TEOS), ethanol, deionized water, and acetic acid in molar ratio equalling 1:4:10:0.5. The prepared sols were dried for several weeks, then the obtained xerogels were further transformed into glass-ceramic materials via the controlled heat treatment at appropriate temperature and time conditions.

The structural characterisation of the fabricated sol-gel materials was provided by X-ray diffraction (XRD) analysis using an X'Pert Pro diffractometer supplied by PANalytical with CuKα radiation with $\lambda = 1.54056$ Å wavelength. The optical properties of the prepared materials were investigated using a Photon Technology International (PTI) Quanta-Master 40 (QM40) UV/VIS Steady State spectrofluorometer equipped with a tunable pulsed optical parametric oscillator (OPO) pumped by the third harmonic of a Nd:YAG laser. The laser system was supplied with a double 200 mm monochromator, a xenon lamp, as well as a multimode UV/VIS PMT detector (R928, PTI Model 914), and a Hamamatsu H10330B-75 detector.

## 3. Results and discussion

### 3.1. Structural studies

XRD studies showed that the heat treatment of the initial xerogels leads to the formation of nano-GCs. The XRD pattern confirmed the crystallization of $LaF_3$ phase in a $P6_3cm$ space group according to ICDD card no. 00-008-0461 [44, 45]. The average size of the precipitated fluoride nanocrystals fluctuates from 8.1 nm [41] to 13.5 nm [43]. Figure 1 presents the diffraction patterns of the sol-gel systems before and after the controlled heat-treatment process. The results from the XRD analysis were confirmed by the transmission electron microscopy (TEM) [41–43].

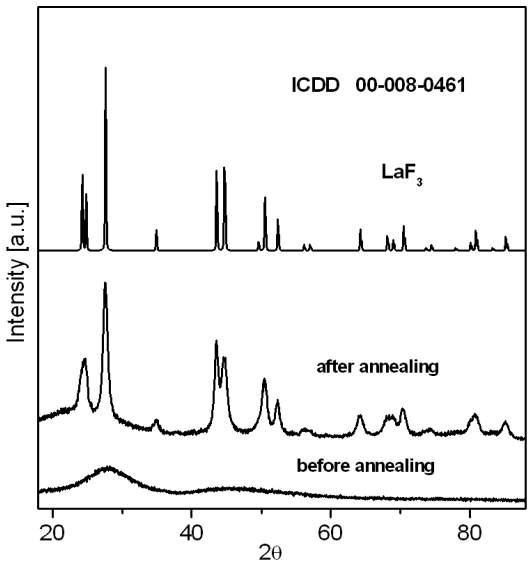


**Fig. 1.** XRD patterns of sol-gel materials before and after the annealing process.

### 3.2. Luminescent studies

Figure 2 illustrates the luminescence spectra of europium ions in xerogels and nano-glass-ceramic-materials. The series of registered luminescence bands assigned to the electronic transitions from the $^5D_0$ state to the lower-lying $^7F_J$ levels ($J = 0$–4) of trivalent $Eu^{3+}$ ions. Notably, two luminescence bands are located in the orange and red spectral ranges, respectively. Those emission bands correspond to the $^5D_0 \rightarrow {}^7F_1$ and the $^5D_0 \rightarrow {}^7F_2$ transitions of $Eu^{3+}$ ions and are also shown in the energy level diagram (Fig. 3).

The intensity ratio of the photoluminescence bands changes due to the heat-treatment process. As a result of annealing the amorphous xerogels, a decrease in a $^5D_0 \rightarrow {}^7F_2$ electric-dipole band intensity was observed; subsequently, the intensity of the band, associated with a magnetic-dipole 5D0 → 7F1 transition significantly increased. The observed changes in the emission spectra profile clearly indicate an increase in local symmetry around $Eu^{3+}$ ions. It also suggests a significant contribution of ionic bonds between the activator ions ($Eu^{3+}$) and their nearest surrounding. These differences in luminescence behavior denoted before and after controlled heat treatment of initial xerogels are strictly related to the successful migration of europium ions (with ionic radius 1.120 Å) into $LaF_3$ nanocrystals (ionic radius of $La^{3+}$: 1.216 Å) [46]. Consequently, a decrease in the luminescence intensity R/O-ratio, according to the $^5D_0 \rightarrow {}^7F_2$ and $^5D_0 \rightarrow {}^7F_1$ bands, was observed [3]. Considering the results, the fabricated materials could be used as red or reddish-orange light emitters for optoelectronic applications [20, 41].

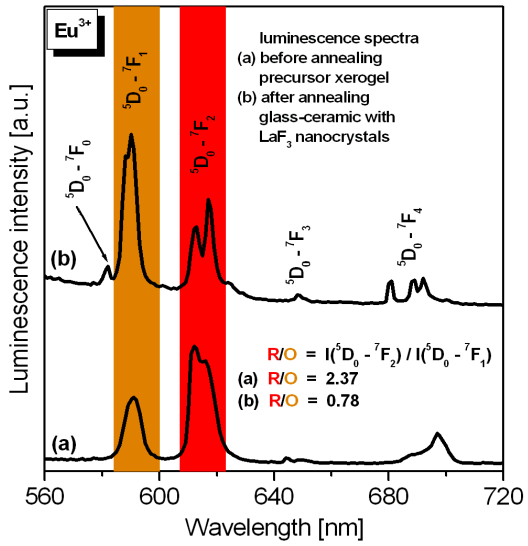


**Fig. 2.** Photoluminescence spectra of $Eu^{3+}$ ions in xerogels and nano-GCs.

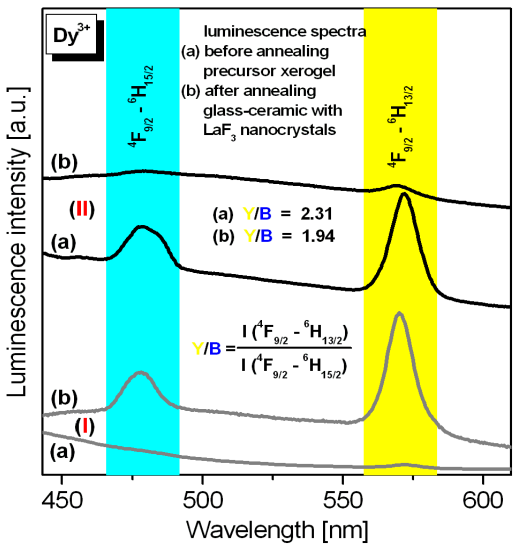


**Fig. 4**. Photoluminescence spectra of $Dy^{3+}$ ions in xerogels and nano-GCs.

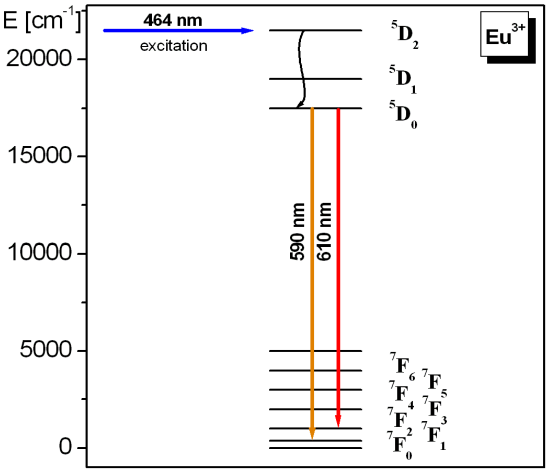


**Fig. 3.** The energy level scheme for $Eu^{3+}$ ions. Orange and red arrows illustrated the major emissions.

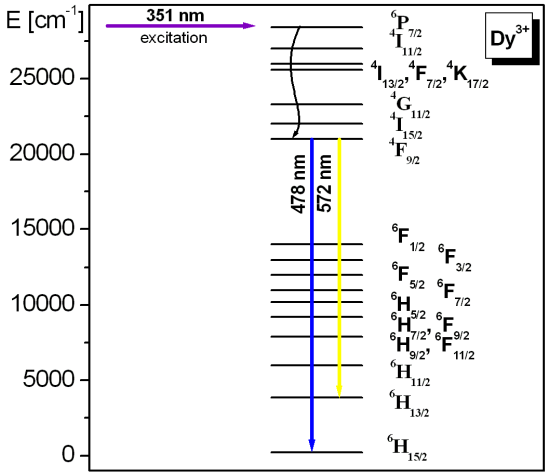


**Fig. 5.** The energy level scheme for $Dy^{3+}$ ions. Blue and yellow arrows illustrated the major emissions.

Figure 4 presents the emission spectra of trivalent dysprosium ions in fabricated sol-gel materials before (xerogel) and after heat treatment (nano-glass-ceramic). The $^4F_{9/2} \rightarrow {}^6H_{15/2}$ and $^4F_{9/2} \rightarrow {}^6H_{13/2}$ transitions of $Dy^{3+}$ ions are located within blue and yellow light spectral ranges, respectively. Those transitions are schematically presented in the energy level scheme (Fig. 5).

The emission spectra were presented for two selected systems, (I) and (II), which differ in the $La^{3+}$:$Dy^{3+}$ ratio, equalling 0.988:0.012 and 0.7:0.3. The results clearly showed that the luminescence properties of $Dy^{3+}$ ions critically depend on the activator concentration [42]. For low $Dy^{3+}$ concentrations (determined by molar ratio $La^{3+}$:$Dy^{3+}$ = 0.988:0.012), the heat-treatment process influenced an increase in the luminescence intensities. Concerning a higher activator concentration (determined by molar ratio $La^{3+}$:$Dy^{3+}$ = 0.7:0.3), the conversely luminescence behavior is observed, and the emission intensity of $Dy^{3+}$ ions is higher for xerogels than for glass-ceramic materials. This phenomenon could be explained by the significant reduction of the inter-ionic distances (and the simultaneous unfavorable increase in interaction) between neighboring $Dy^{3+}$-$Dy^{3+}$ ions inside $LaF_3$ nanocrystals, leading to the concentration quenching of the luminescence. Similarly as for $Eu^{3+}$ ions, a decrease in the calculated Y/B-ratio values (associated with the $^4F_{9/2} \rightarrow {}^6H_{13/2}$ and $^4F_{9/2} \rightarrow {}^6H_{15/2}$ band intensities of $Dy^{3+}$ ions) is noted. The values of both R/O ($Eu^{3+}$) and Y/B ($Dy^{3+}$) ratios are lower for nano-GCs compared to those denoted for the initial xerogels and other inorganic oxide glasses synthesized by the conventional melt-quenching method [47, 48], indicating incorporation of $Ln^{3+}$ ions inside the $LaF_3$ nanocrystalline phase. However, it should be clarified that the denoted decrease in Y/B ratio is not as noticeable as for R/O ratio ($Eu^{3+}$), suggesting less efficient migration of $Dy^{3+}$ into $LaF_3$ nanocrystals. Such a result could be explained by greater differences in ionic radii in $Dy^{3+}$ (1.083 Å) - $La^{3+}$ (1.216 Å) pair than in $Eu^{3+}$ (1.120 Å) - $La^{3+}$ (1.216 Å) one [46]. The results suggest that the obtained GCs could find application as visible light emitters [22, 42].

Figure 6 presents the photoluminescence spectra recorded for the sol-gel materials doped with $Pr^{3+}$ ions. For xerogel, none of the characteristic luminescence bands

were observed. The probable reason for this observation is correlated with too small energy gaps between the appropriate states of $Pr^{3+}$ ions and the presence of high-vibrational energy hydroxyl groups. The vibrations of $OH^-$ groups overlap with the gaps between $Pr^{3+}$ states, which is responsible for effectively quenching the photoluminescence. It should be noted that for xerogel, only a broad band was registered. Based on the literature, this broad band could be originated from defects inside the sol-gel host [49]. The effect of photon recombination in the silicate sol-gel host could be reduced or disappear after the thermal treatment. Conversely, the spectrum recorded for the nano-glass-ceramic material revealed the well-visible emission bands within the blue, green, and red ranges, assigned to the characteristic transitions of $Pr^{3+}$ ions, i.e., $^3P_0 \rightarrow {}^3H_4$, $^3P_1 \rightarrow {}^3H_5$, $^3P_0 \rightarrow {}^3H_5$, $^3P_0 \rightarrow {}^3H_6$, $^1D_2 \rightarrow {}^3H_4$, and $^3P_0 \rightarrow {}^3F_2$ (Fig. 7). Since the intensities of emission bands from the $^3P_{0,1}$ levels are enhanced, it could be expected that $Pr^{3+}$ ions are well-incorporated inside precipitated LaF3 nanocrystals. Indeed, there are differences in ionic radii between $Pr^{3+}$ (1.179 Å) and $La^{3+}$ (1.216 Å), compared to other $Eu^{3+}$-$La^{3+}$ and $Dy^{3+}$-$La^{3+}$ ionic pairs [46]. It is worth noting that in the case of the studied $Pr^{3+}$-doped GCs, the combination of blue, green, and reddish-orange luminescence is appropriate for white light generation, described by chromaticity coordinates (0.400|0.337) and correlated colour temperature equal to 3124 K [43].

Furthermore, the decay analysis from the appropriate excited states of studied $Ln^{3+}$ ions was also performed. The lifetimes of the $^5D_0$ ($Eu^{3+}$) and the $^4F_{9/2}$ ($Dy^{3+}$) levels were determined both for xerogels and glass-ceramic materials after controlled heat-treatment process. The resultant values were collected in Table 1.

**Table 1.**
The lifetimes of appropriate excited states of $Ln^{3+}$ ions estimated for xerogles and nano-GCs.

| $Ln^{3+}$ | Excited state | Luminescence lifetimes (ms) | |
|---|---|---|---|
| $Eu^{3+}$ | $^5D_0$ | xerogels | 0.22 |
| | | nano-GCs | 0.79<br>9.76 |
| $Dy^{3+}$ | $^4F_{9/2}$ | xerogels | 0.027 |
| | | nano-GCs | 0.034<br>1.731 |

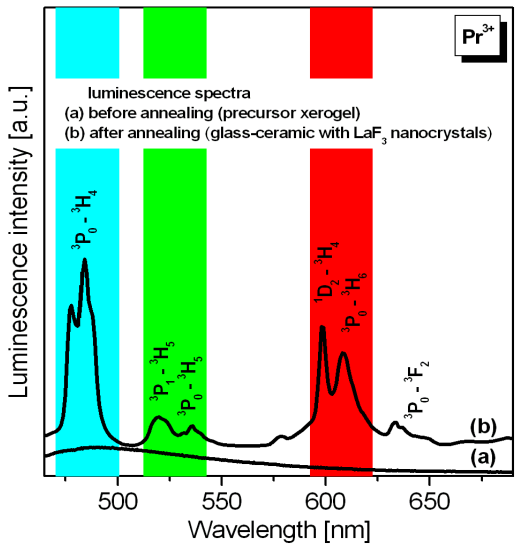


**Fig. 6.** Photoluminescence spectra of $Pr^{3+}$ ions in xerogels and GCs.

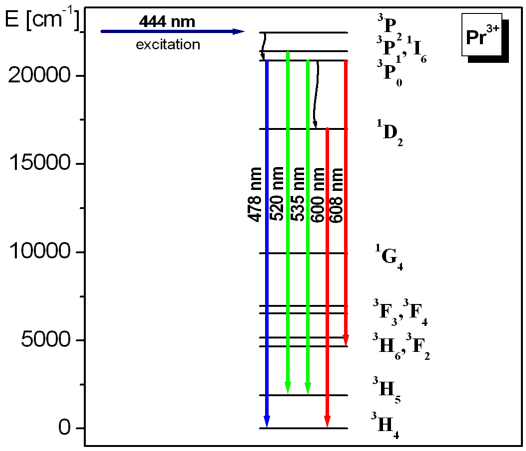


**Fig. 7.** The energy level scheme for $Pr^{3+}$ ions. The major emissions were illustrated by blue, green, and red arrows.

Conversely to the initial xerogels, the photoluminescence decay curves recorded for nano-GCs exhibited a biexponential character. The curve with shorter and longer decay components is associated with the distribution of $Eu^{3+}$ and $Dy^{3+}$ ions between the amorphous sol-gel host and the nanocrystalline fluoride phase. The obtained results clearly showed that the overall emission and luminescence lifetimes are significantly enhanced for nano-glass-ceramic systems containing $LaF_3$ nanocrystals compared with initial fully amorphous xerogels.

## 4. Conclusions

This paper presents the selected research results for xerogels and nano-glass-ceramic materials fabricated by the sol-gel technology. The emission characterisation was conducted for samples doped with selected $Ln^{3+}$ ions, i.e., $Eu^{3+}$, $Dy^{3+}$, and $Pr^{3+}$ ions.

The results revealed that for prepared nano-glass-ceramic materials, the luminescence intensities are noticeably enhanced and the decay times are prolonged ($^5D_0$ ($Eu^{3+}$): $\tau_1 = 0.79$ ms, $\tau_2 = 9.76$ ms; $^4F_{9/2}$ ($Dy^{3+}$): $\tau_1 = 0.034$ ms, $\tau_2 = 1.731$ ms) compared to the initial xerogels ($^5D_0$ ($Eu^{3+}$): $\tau = 0.22$ ms; $^4F_{9/2}$ ($Dy^{3+}$): $\tau = 0.027$ ms). This phenomenon could be explained by successfully entering trivalent $Ln^{3+}$ ions inside $LaF_3$ nanocrystal lattice, formed during a heat treatment of xerogels. A decrease in the values of the R/O-(xerogel: 2.37, GC: 0.78) and Y/B-ratio (xerogel: 2.31, GC: 1.94) also indicates the migration of the dopant ions into the crystalline phase. The studies demonstrated the impact of $LaF_3$ nanocrystals dispersed in a sol-gel host on the photoluminescence properties of $Eu^{3+}$, $Dy^{3+}$, and $Pr^{3+}$ ions. The luminescence behaviour also depends on the activator concentration, similarity in ionic radius in individual $Ln^{3+}$-$La^{3+}$ pair, and individual distribution of the energy levels.

Nano-glass-ceramic materials obtained by the sol-gel method are promising systems able to generate visible light and may find applications in photonics, like optical hosts

for multicolour displays or colour screens. Indeed, $Eu^{3+}$-doped GCs can generate red or reddish-orange luminescence, while $Dy^{3+}$-doped samples produce efficiently yellow light. Importantly, in the case of $Pr^{3+}$-doped GCs, the intensities of blue, green, and reddish-orange emissions are relevant for warm-white light generation.

## Authors' statement

Research concept and design, W.A.P.; collection and/or assembly of data, J.Ś. and N.P.; data analysis and interpretation, J.Ś. and N.P.; writing the article, J.Ś., N.P., and W.A.P.; critical revision of the article, W.A.P, J.P., and N.P.; final approval of article, W.A.P. and J.P.

## Acknowledgements

The research activities are co-financed by the funds granted under the Research Excellence Initiative of the University of Silesia in Katowice, Poland.

## References

[1] Beall, G. H. Dr. S. Donald (Don) Stookey (1915–2014): Pioneering Researcher and Adventurer. *Front. Mater.* **3**, 37 (2016). https://doi.org/10.3389/fmats.2016.00037

[2] Beall, G. H. & Duke, D. A. Transparent glass-ceramics. *J. Mater. Sci.* **4**, 340–352 (1969). https://doi.org/10.1007/BF00550404

[3] Beall, G. H. & Pinckney, L. R. Nanophase glass-ceramics. *J. Am. Ceram. Soc.* **82**, 5–16 (1999). https://doi.org/10.1111/j.1151-2916.1999.tb01716.x

[4] Beall, G. H. Milestones in glass-ceramics: A personal perspective. *Int. J. Appl. Glass Sci.* **5**, 93–103 (2014). https://doi.org/10.1111/ijag.12063

[5] Sakamoto, A. & Yamamoto, S. Glass-ceramics: Engineering principles and applications. *Int. J. Appl. Glass Sci.* **1**, 237–247 (2010). https://doi.org/10.1111/j.2041-1294.2010.00027.x

[6] Sołtys, M., Górny, A., Pisarska, J. & Pisarski, W. A. Electrical and optical properties of glasses and glass-ceramics. *J. Non-Cryst. Solids* **498**, 352–363 (2018). https://doi.org/10.1016/j.jnoncrysol.2018.03.033

[7] Soares, V. O. *et al*. Highly translucent nanostructured glass-ceramic. *Ceram. Int.* **47**, 4707–4714 (2021). https://doi.org/10.1016/j.ceramint.2020.10.039

[8] Zanotto, E. D. A bright future for glass-ceramics. *Am. Ceram. Soc. Bull.* **89**, 19–27 (2010). https://ceramics.org/wp-content/uploads/2010/09/bulletin_oct-nov2010.pdf

[9] Montazerian, M., Singh, S. P. & Zanotto, E. D. An analysis of glass–ceramic research and commercialization. *Am. Ceram. Soc. Bull.* **94**, 30–35 (2015). https://lamav.weebly.com/uploads/5/9/0/2/5902800/an_analysis_of_glass-ceramic.pdf

[10] Deubener, J. *et al*. Updated definition of glass-ceramics. *J. Non-Cryst. Solids* **501**, 3–10 (2018). https://doi.org/10.1016/j.jnoncrysol.2018.01.033

[11] Gonçalves, M. C., Santos, L. F. & Almeida, R. M. Rare-earth-doped transparent glass ceramics. *C. R. Chim.* **5**, 845–854 (2002). https://doi.org/10.1016/S1631-0748(02)01457-1

[12] Ren, J., Lu, X., Lin, C. & Jain, R. K. Luminescent ion-doped transparent glass ceramics for mid-infrared light sources. *Opt. Exp.* **28**, 21522–21548 (2020). https://doi.org/10.1364/OE.395402

[13] Pisarski, W. A. *et al.* Rare earth-doped lead borate glasses and transparent glass-ceramics: Structure–property relationship. *Spectrochim. Acta A* **79**, 696–700 (2011). https://doi.org/10.1016/j.saa.2010.04.022

[14] Marcondes, L. M. *et al*. $Er^{3+}$-doped niobium alkali germanate glasses and glass-ceramics: NIR and visible luminescence properties. *J. Non-Cryst. Solids* **521**, 119492 (2019). https://doi.org/10.1016/j.jnoncrysol.2019.119492

[15] Lahoz, F. *et al*. Rare earths in nanocrystalline glass-ceramics. *Opt. Mater.* **27**, 1762–1770 (2005). https://doi.org/10.1016/j.optmat.2004.11.047

[16] Li, Z. *et al*. The transformation from translucent into transparent rare earth ions doped oxyfluoride glass-ceramics with enhanced luminescence. *Adv. Opt. Mater.* **10**, 2102713 (2022). https://doi.org/10.1002/adom.202102713

[17] Cruz, M. E. *et al*. Rare-earth doped transparent oxyfluoride glass-ceramics: processing is the key. *Opt. Mater. Exp.* **12**, 3493–3516 (2022). https://doi.org/10.1364/OME.462684

[18] Patra, P. *et al.* The effect of rare earth ($RE^{3+}$) ionic radii on transparent lanthanide-tellurite glass-ceramics: correlation between 'hole-formalism' and crystallization. *Mater. Adv.* **4**, 2667–2682 (2023). https://doi.org/10.1039/D3MA00036B

[19] Yuhang, X. *et al*. Luminescence properties of $Eu^{3+}$ doped $BaMoO_4$ transparent glass ceramics. *J. Non-Cryst. Solids* **500**, 243–248 (2018). https://doi.org/10.1016/j.jnoncrysol.2018.08.007

[20] Desirena, H. *et al*. $Eu^{3+}$ heavily doped tellurite glass ceramic as an efficient red phosphor for white LED. *J. Lumin.* **250**, 11980 (2022). https://doi.org/10.1016/j.jlumin.2022.119080

[21] Bondzior, B., Hoang, T. & Petit, L. Crystal formation in $Eu^{3+}$-Doped oxyfluorophosphate glass-ceramics for luminescence thermometry. *Ceram. Int.* **49**, 41186–41193 (2023). https://doi.org/10.1016/j.ceramint.2023.04.155

[22] Wang, L. *et al.* Luminescence properties of $Dy^{3+}$ doped glass ceramics containing $Na_3Gd(PO_4)_2$. *J. Non-Cryst. Solids* **543**, 120091 (2020). https://doi.org/10.1016/j.jnoncrysol.2020.120091

[23] Yan, Y. *et al*. Preparation and luminescence of $Dy^{3+}$ doped glass-ceramics containing $ZnMoO_4$. *J. Non-Cryst. Solids* **569**, 120990 (2021). https://doi.org/10.1016/j.jnoncrysol.2021.120990

[24] Jia, F. *et al.* Effect of $Mg^{2+}$/$Sr^{2+}$ addition on luminescence properties of $Dy^{3+}$ doped glass ceramics containing $Ca_2Ti_2O_6$. *Opt. Mater.* **131**, 112715 (2022). https://doi.org/10.1016/j.optmat.2022.112715

[25] Bu, Y. Y, Cheng, S. J., Wang, X. F. & Yan, X. H. Optical thermometry based on luminescence behavior of $Dy^{3+}$-doped transparent $LaF_3$ glass ceramics. *Appl. Phys. A* **121**, 1171–1178 (2015). https://doi.org/10.1007/s00339-015-9483-7

[26] Lee, H., Chung, W. J. & Im, W. B. $Pr^{3+}$-doped oxyfluoride glass ceramic as a white LED color converter wide color gamut. *J. Lumin.* **236**, 118064 (2021). https://doi.org/10.1016/j.jlumin.2021.118064

[27] Chen, Z. *et al.* Tailorable upconversion white light emission from $Pr^{3+}$ single-doped glass ceramics via simultaneous dual-lasers excitation. *Adv. Opt. Mater.* **6**, 1700787 (2018). https://doi.org/10.1002/adom.201700787

[28] Hu, X. *et al*. Opposite temperature luminescent behaviours of $Tb^{3+}$ and $Pr^{3+}$ co-doped $BaMoO_4$ glass ceramics for temperature sensing. *J. Lumin.* **236**, 118080 (2021). https://doi.org/10.1016/j.jlumin.2021.118080

[29] Liu, W. *et al*. Structure and luminescence of $Pr^{3+}$-doped oxyfluoride glass-ceramics containing $Na_5Y_9F_{32}$:$Pr^{3+}$ nanocrystals. *J. Lumin.* **267**, 120404 (2024). https://doi.org/10.1016/j.jlumin.2023.120404

[30] Zhang, W. J. *et al.* Near-infrared quantum splitting in $Ho^{3+}$:$LaF_3$ nanocrystals embedded germanate glass ceramic. *Opt. Mater. Exp.* **2**, 636–643 (2012). https://doi.org/10.1364/OME.2.000636

[31] Chen, D., Wang, Y., Yu, Y. & Ma, E. Influence of $Yb^{3+}$ content on microstructure and fluorescence of oxyfluoride glass ceramics containing $LaF_3$ nano-crystals. *Mater. Chem. Phys.* **101**, 464–469 (2007). https://doi.org/10.1016/j.matchemphys.2006.08.005

[32] Tanabe, S., Hayashi, H., Hanada, T. & Onodera, N. Fluorescence properties of $Er^{3+}$ ions in glass ceramics containing $LaF_3$ nanocrystals. *Opt. Mater.* **19**, 343–349 (2002). https://doi.org/10.1016/S0925-3467(01)00236-1

[33] Chen, Z. *et al.* Improved up-conversion luminescence from $Er^{3+}$:$LaF_3$ nanocrystals embedded in oxyfluoride glass ceramics via simultaneous triwavelength excitation. *J. Phys. Chem. C* **119**, 24056–24061 (2015). https://doi.org/10.1021/acs.jpcc.5b08103

[34] Chen, Z. *et al.* Near-infrared wavelength-dependent nonlinear transmittance tailoring in glass ceramics containing $Er^{3+}$:$LaF_3$ nanocrystals. *J. Mater. Chem. C* **4**, 6707–6712 (2016). https://doi.org/10.1039/C6TC01876A

[35] Gorni, G. *et al*. $80SiO_2$-$20LaF_3$ oxyfluoride glass ceramic coatings doped with $Nd^{3+}$ for optical applications. *Int. J. Appl. Glass Sci.* **9**, 208–217 (2018). https://doi.org/10.1111/ijag.12338

[36] Sedano, M. *et al*. Luminescence of $Nd^{3+}$-doped $LaF_3$ glass-ceramics enhanced with Ag nanoparticles. *J. Eur. Ceram. Soc.* **44**, 2427–2436 (2024). https://doi.org/10.1016/j.jeurceramsoc.2023.11.029

[37] Xu, Y. *et al*. Efficient near-infrared down-conversion in $Pr^{3+}$-$Yb^{3+}$ codoped glasses and glass ceramics containing $LaF_3$ nanocrystals. *J. Phys. Chem. C* **115**, 13056–13062 (2011). https://doi.org/10.1021/jp201503v

[38] Secu, M., Secu, C. & Bartha, C. Optical properties of transparent rare-earth doped sol-gel derived nano-glass ceramics. *Materials* **14**, 6871 (2021). https://doi.org/10.3390/ma14226871

[39] Rodriguez, V. D. *et al*. Luminescence of $Er^{3+}$-doped nanostructured $SiO_2$-$LaF_3$ glass-ceramics prepared by the sol-gel method. *Opt. Mater.* **29**, 1557–1561 (2007). https://doi.org/10.1016/j.optmat.2006.06.022

[40] Cruz, M. E. *et al*. A new sol-gel route towards $Nd^{3+}$-doped $SiO_2$–$LaF_3$ glass-ceramics for photonic applications. *Mater. Adv.* **1**, 3589–3596 (2020). https://doi.org/10.1039/d0ma00708k

[41] Pawlik, N., Szpikowska-Sroka, B., Pietrasik, E., Goryczka, T. & Pisarski, W. A. Structural and luminescence properties of silica powders and transparent glass-ceramics containing $LaF_3$:$Eu^{3+}$ nanocrystals. *J. Am. Ceram. Soc.* **101**, 4654–4668 (2018). https://doi.org/10.1111/jace.15728

[42] Pawlik, N., Goryczka, T., Pietrasik, E., Śmiarowska, J. & Pisarski, W. A. Photoluminescence investigations of $Dy^{3+}$-doped silicate xerogels and $SiO_2$-$LaF_3$ nano-glass-ceramic materials. *Nanomaterials* **12**, 4500 (2022). https://doi.org/10.3390/nano12244500

[43] Pawlik, N., Goryczka, T., Zubko, M., Śmiarowska, J. & Pisarski, W. A. White light and near-infrared emissions of $Pr^{3+}$ ions in $SiO_2$-$LaF_3$ sol-gel nano-glass-ceramics. *Nanoscale* **16**, 4249–4265 (2024). https://doi.org/10.1039/d3nr04030e

[44] Hémono, N. *et al*. Processing of transparent glass-ceramics by nanocrystallisation of $LaF_3$. *J. Eur. Ceram. Soc.* **29**, 2915–2920 (2009). https://doi.org/10.1016/j.jeurceramsoc.2009.05.013

[45] de Pablos-Martín, A. *et al*. Crystallization kinetics of $LaF_3$ nanocrystals in an oxyfluoride glass. *J. Am. Ceram. Soc.* **94**, 2420–2428 (2011). https://doi.org/10.1111/j.1551-2916.2011.04547.x

[46] D'Angelo, P. *et al*. Revised ionic radii of lanthanoid(III) ions in aqueous solution. *Inorg. Chem.* **50**, 4572–4579 (2011). https://doi.org/10.1021/ic200260r

[47] Pisarski, W. A., Żur, L. & Pisarska, J. Optical transitions of $Eu^{3+}$ and $Dy^{3+}$ ions in lead phosphate glasses. *Opt. Lett.* **36**, 990–992 (2011). https://doi.org/10.1364/OL.36.000990

[48] Pisarski, W. A., Pisarska, J., Żur, L. & Goryczka, T. Structural and optical aspects for $Eu^{3+}$ and $Dy^{3+}$ ions in heavy metal glasses based on $PbO$-$Ga_2O_3$-$XO_2$ (X = Te, Ge, Si). *Opt. Mater.* **35**, 1051–1056 (2013). https://doi.org/10.1016/j.optmat.2012.12.012

[49] Kłonkowski, A. M., Wiczk, W., Ryl, J., Szczodrowski, K. &Wileńska, D. A white phosphor based on oxyfluoride nano-glass-ceramics co-doped with $Eu^{3+}$ and $Tb^{3+;}$ Energy transfer study. *J. Alloys Compd.* **724**, 649–658 (2017). https://doi.org/10.1016/j.jallcom.2017.07.055